JCTC Journal of Chemical Theory and Computation

Effects of Peripheral Substituents on the Electronic Structure and Properties of Unligated and Ligated Metal Phthalocyanines, Metal = Fe, Co, Zn

Meng-Sheng Liao,[†,§] John D. Watts,[†] Ming-Ju Huang,*[,†] Sergiu M. Gorun,[‡] Tapas Kar,[§] and Steve Scheiner*[,§]

Department of Chemistry, P.O. Box 17910, Jackson State University, Jackson, Mississippi 39217, Department of Chemistry and Environmental Science, New Jersey Institute of Technology, Newark, New Jersey 07102, and Department of Chemistry and Biochemistry, Utah State University, Logan, Utah 84322-0300

Received April 18, 2005

Abstract: The effects of peripheral, multiple −F as well as $-C_2F_5$ substituents, on the electronic structure and properties of unligated and ligated metal phthalocyanines, PcM, PcM(acetone)$_2$ (M = Fe, Co, Zn), PcZn(Cl), and PcZn(Cl^-), have been investigated using a DFT method. The calculations provide a clear explanation for the changes in the ground state, molecular orbital (MO) energy levels, ionization potentials (IP), electron affinities (EA), charge distribution on the metal (Q_M), axial binding energies, and in electronic spectra. While the strongly electron-withdrawing $-C_2F_5$ groups on the Pc ring change the ground state of PcFe, they do not influence the ground state of PcCo. The IP is increased by ∼1.3 eV from H_{16}PcM to F_{16}PcM and by another ∼1.1 eV from F_{16}PcM to F_{48}PcM. A similar increase in the EA is also found on going from H_{16}PcM to F_{48}PcM. Substitution by the $-C_2F_5$ groups also considerably increases the binding strength between PcM and the electron-donating axial ligand(s). Numerous changes in chemical and physical properties observed for the F_{64}PcM compounds can be accounted for by the calculated results.

1. Introduction

Metal phthalocyanines (PcMs), with their planar square structure, are interesting molecules that have been studied extensively in the literature. (Pc is used here to refer to any phthalocyanine, regardless of substituents.) They provide a versatile chemical system: almost every metal in the periodic table can combine with the Pc ring, and most of these compounds are very stable. The diversity of phthalocyanines, together with their high thermal and chemical stability, has made them suitable for many technological applications such as dyes, pigments, semiconductors,[1] energy conversion (photovoltaic and solar cells),[2] electrophotography,[3] photosensitizers,[4] gas sensors,[5] low-dimensional metals,[6] electrochromism,[7] Langmuir−Blodgett (LB) films,[8] liquid crystals,[9] and nonlinear optics.[10]

Consequently, a great deal of effort has been expended to develop new phthalocyanine materials that display certain characteristics useful for the particular application. It has been shown that the properties of phthalocyanines can be effectively modulated with different substituents on the periphery of the macrocycle. A useful methodology is the replacement of the hydrogens (Hs) of Pc with halogens (Xs), which can greatly increase the catalytic activity and stability of PcMs.[11,12] However, halogenated PcMs have the disadvantage of poor solubility, which impedes many new applications of the materials. Recently, several novel octakis-(perfluoro *i*-C_3F_7)(perfluoro)-PcM compounds (F_{64}PcM) (M = Zn, Co, Fe) have been synthesized and characterized by one of us,[13−16] where the aromatic X-atoms of halogenated

* Corresponding author e-mail: scheiner@cc.usu.edu.
† Jackson State University.
‡ New Jersey Institute of Technology.
§ Utah State University.

10.1021/ct050105y CCC: $30.25
Published on Web 08/27/2005

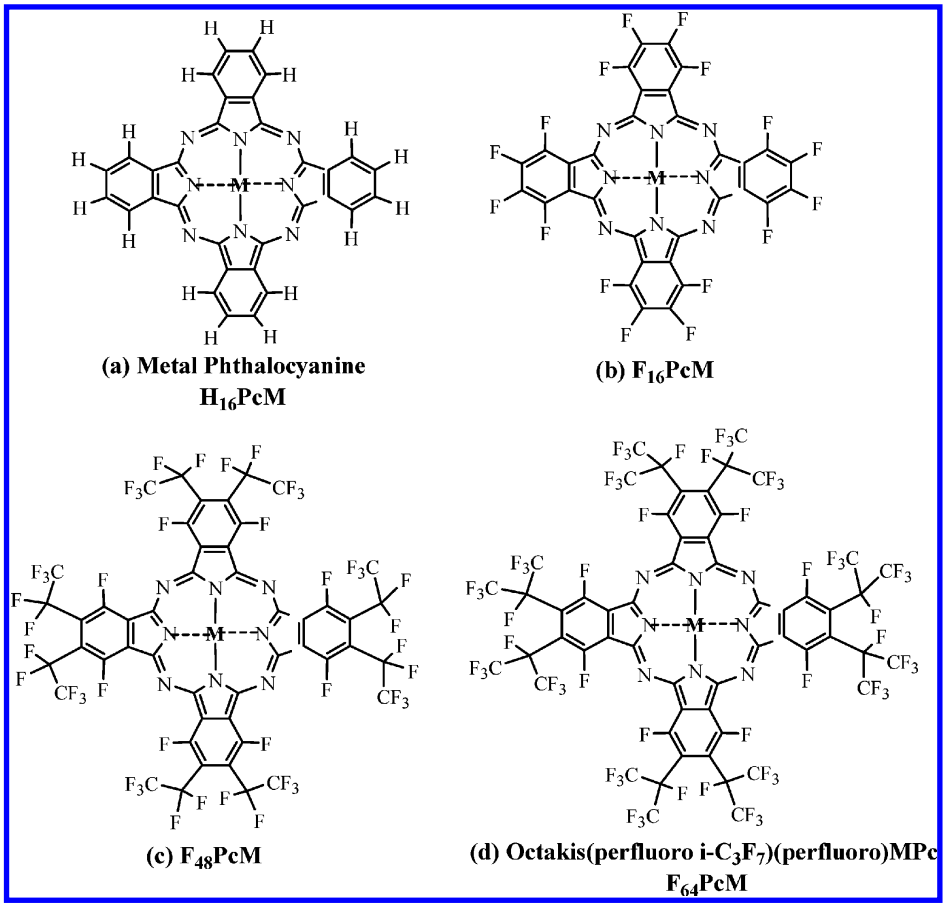

Figure 1. Molecular structures of metal phthalocyanine (H_{16}PcM) and its fluorosubstituted derivatives.

PcM (X_{16}PcM) are partially replaced by perfluoro isopropyl (*i*-C_3F_7) groups (R_f). These R_f groups are much more electronegative than the F atoms and were shown to increase the solubility of the compounds and also promote novel catalytic oxidations while resisting self-oxidation.[13]

In a recent paper,[17] density functional theory (DFT) calculations were carried out to investigate the electronic structure and properties of unligated and ligated F_{64}PcFe complexes. One important observation was the change of the ground state of Fe^{II} caused by the strongly electron-withdrawing peripheral substituents at the Pc ring. To shed more light on the effects of the R_f substituents, the previous theoretical study is extended in this report to include systems where M, Co, or Zn is four-, five-, or six-coordinated.

F_{64}PcZn has been studied in detail using single-crystal X-ray diffraction, optical and photoacoustic spectroscopy, and cyclic voltammetry, and it exhibits a number of interesting properties. (1) The ultraviolet−visible (UV−vis) spectra of F_{64}PcZn differ significantly from those of the parent, unsubstituted H_{16}PcZn species,[13] indicating that the electron-withdrawing property of the peripheral substituents affects the ring π molecular orbitals (MOs) to differing extents. (2) There are large shifts in the ring redox (oxidation and reduction) potentials on going from H_{16}PcZn to F_{64}PcZn, and the increase in oxidation potentials provides extra stability toward oxidative destruction for the R_f-substituted phthalocyanine.[13] (3) It is difficult to photochemically oxidize F_{64}PcZn, in stark contrast with the behavior of H_{16}PcZn, for which the photooxidation reaction results in the formation of a $[H_{16}PcZn]^+$ species.[13] (4) Axial ligation to F_{64}PcZn is favored relative to H_{16}PcZn; the X-ray structure of the former complex reveals the formation of $F_{64}PcZn(Ace)_2$ (Ace = acetone), but H_{16}PcZn as well as F_{16}PcZn do not retain solvent when crystallized.[14] Anionic ligands such as Cl^-, coordinate even more strongly. Thus, electrospray ionization mass spectrometry data for a DMF solution of F_{64}PcZn indicated the existence of F_{64}PcZn(Cl) and $F_{64}PcZn(Cl^-)$.[13]

The main goals of the present report are to examine the effects of F^- and R_f-substituents on various properties that include electronic structure, oxidation/reduction properties, ionization potentials, electron affinities, etc. This work extends previous semiempirical ZINDO and MOPAC calculations on F_{64}PcZn,[13] which were aimed mainly at interpretation of the absorption spectra of the metal complexes. The axial bonding properties of acetone, Cl, or Cl^- to the metal complexes are also examined. For comparison among the different metals, the results of iron phthalocyanines are also reported here.

2. Computational Details

The molecular structure of the parent metal phthalocyanine H_{16}PcM is illustrated in Figure 1a and that of (perfluoro *i*-C_3F_7)-(perfluoro)phthalocyanine, F_{64}PcM, is in Figure 1d. For computational convenience, the isopropyl $-C_3F_7$ substituent was modeled by ethyl $-C_2F_5$. The use of the smaller F_{48}PcM (Figure 1c) as an accurate electronic mimic of the larger F_{64}PcM was demonstrated in our previous calculations.[17] This simplification is also supported by earlier

semiempirical ZINDO calculations,[13] which show that the spectrum predicted for F_{48}PcZn is almost identical to that of F_{64}PcZn. For the sake of comparison and completion, the parent perfluorinated metal phthalocyanines, F_{16}PcM (Figure 1b), have also been considered here.

All calculations were carried out using the Amsterdam Density Functional (ADF) program package (version 2000.02) developed by Baerends and co-workers.[18−21] A triple-ζ STO basis was used for the metal 3s−4s shells plus one 4p polarization function, a triple-ζ basis for C/N/O 2s−2p and Cl 3s−3p shells plus one 3d polarization function, a double-ζ basis for F 2s−2p shells, and a double-ζ basis for the H 1s shell. It has been shown that high-quality basis sets (triple-ζ plus one polarization function) are required for the atoms within the macrocycle ring of the phthalocyanine in order to obtain the correct ground states of H_{16}PcFe and its derivatives.[22] The inner orbitals, i.e., 1s−2p for Fe/Cl and 1s for C/N/O/F, were considered as core and kept frozen according to the frozen-core approximation.[18] Among the various exchange-correlation potentials available, the density-parametrization form of Vosko, Wilk, and Nusair (VWN)[23] plus Becke's gradient correction for exchange (B)[24] and Perdew's gradient correction for correlation (P)[25] were employed. The combined VWN-B-P functional has been shown to provide accurate bonding energies for both main-group[26] and transition metal[27] systems. Relativistic corrections of the valence electrons were calculated by the quasi-relativistic (QR) method.[28] For the open-shell states, the unrestricted Kohn−Sham (UKS) spin-density functional approach was adopted.

Electron excitation energies related to the electronic absorption spectra were calculated using the time-dependent density functional response theory (TDDFT)[29] as implemented in the ADF program. TDDFT provides a first-principles method for the calculation of excitation energies and presents an excellent alternative to the conventional highly correlated configuration interactions (CI) method. Applications of TDDFT to excitation energy calculations can be found in recent work.[30,31]

3. Results and Discussion

Unsubstituted transition-metal H_{16}PcMs have been shown to have square planar D_{4h} symmetry.[30] X-ray crystal structure data[13−16] indicate that the Pc ring in substituted F_{64}PcM is quite planar, and this ring planarity is maintained in the solid state even in the presence of axial acetone ligands. The solution UV−vis spectra[32a−c,33] are also consistent with D_{4h} symmetry. The invariability of the MN_4 chromophore geometry upon substitution of the peripheral H-atoms by *i*-C_3F_7 groups strongly suggests that the geometry will not change for steric reasons when the *i*-C_3F_7 groups are replaced by less bulky groups in F_{16}PcM and F_{48}PcM. This argument is indeed supported by calculations.[13] Placing the molecule in the *xy* plane, the five metal 3d-orbitals transform as a_{1g} (d_{z^2}), b_{1g} ($d_{x^2-y^2}$), b_{2g} (d_{xy}), and e_g (d_π, i.e., d_{xz} and d_{yz}). For Fe^{II} and Co^{II}, different occupations of electrons in these d-orbitals may yield a number of possible low-lying states. To determine the ground state, relative energies of several selected configurations in H_{16}PcM, F_{16}PcM, and F_{48}PcM (M = Fe, Co) were calculated, wherein geometry optimization was performed separately for each state considered. These energies are reported in Table 1, along with the optimized M−N bond lengths.

Table 1. Calculated Relative Energies (*E*, eV) for Selected Configurations in H_{16}PcM, F_{16}PcM, and F_{48}PcM (M = Fe, Co)

configuration[a]				*E* (R)[b]		
b_{2g}/d_{xy}	a_{1g}/d_{z^2}	$1e_g$/d_π	state	H_{16}PcM	F_{16}PcM	F_{48}PcM
				M = Fe[c]		
2	2	2	$^3A_{2g}$	**0** (1.916)	**0** (1.918)	0 (1.919)
2	1	3	^3E_g (A)	0.05 (1.923)	0.01 (1.922)	−0.04 (1.921)
1	1	4	$^3B_{2g}$	0.08 (1.921)	0.05 (1.919)	**−0.06** (1.917)
1	2	3	^3E_g (B)	0.52 (1.910)	0.52 (1.911)	0.45 (1.910)
2	0	4	$^1A_{1g}$	1.43 (1.935)	1.37 (1.934)	1.28 (1.933)
				M = Co		
2	1	4	$^2A_{1g}$	**0** (1.922)	**0** (1.924)	**0** (1.931)
2	2	3	^2E_g	0.21 (1.909)	0.24 (1.911)	0.28 (1.916)
1	2	4	$^2B_{2g}$	0.95 (1.901)	0.94 (1.904)	0.88 (1.904)

[a] Orbital energy levels illustrated in Figure 2. [b] Values in parentheses refer to optimized M−N(Pc) bond length (in Å) for the pertinent state. [c] The calculated *E*'s and *R*'s with the present version ADF program (2000.02) may be slightly different from those obtained with the older version ADF (2.0.1), ref 17, but the trends of the results are not changed.

Table 2 displays the gross populations of M 3d, 4s, and 4p orbitals (in the ground state), along with the metal's Mulliken atomic charge. Table 3 lists the calculated M−Pc binding energies (E_{bind}), ionization potentials (IP) for several outer MOs, and the electron affinities (EA). E_{bind} is defined as the energy required to pull the metal apart from the Pc ring

$$-E_{bind} = E(\mathrm{PcM}) - \{E(\mathrm{M}) + E(\mathrm{Pc})\}$$

where *E*(PcM), *E*(M), and *E*(Pc) represent the total energies of the indicated species. (The geometries of PcM and Pc are independently optimized.) The IPs and EAs were calculated by the so-called ΔSCF method which carries out separate SCF (self-consistent field) calculations for the neutral molecule and its ion, where $EA = E(X^-) - E(X)$. The computed relative energies of selected configurations of the ligated iron phthalocyanines are contained in Table 4, and their properties are presented in Table 5.

The electronic structure of H_{16}PcFe has been the subject of several experimental studies.[34−36] A $^3B_{2g}$ ground state was originally suggested for H_{16}PcFe on the basis of magnetic work,[35] but later magnetic circular dichroism spectra have shown that the ground state is in fact $^3A_{2g}$.[36] Our previous calculations[37] support the latter assignment. In a recent paper of ours,[17] we further calculated F_{16}PcFe, F_{48}PcFe, and their complexes with two axial ligands L (L = Ace, H_2O, pyridine). It is shown that the electronic configuration of each ligated PcFe is determined mainly by the axial ligand-field strength but can also be affected by peripheral substituents. Figure 2 illustrates the changes of the electronic structure from H_{16}PcFe to F_{16}PcFe to F_{48}PcFe. A detailed discussion of the results for the iron−phthalocyanine complexes is reported in ref 17.[38]

Table 2. Mulliken Orbital Populations and Atomic Charges on Metal (Q_M)

	H_{16}PcFe	F_{16}PcFe	F_{48}PcFe	H_{16}PcCo	F_{16}PcCo	F_{48}PcCo	H_{16}PcZn	F_{16}PcZn	F_{48}PcZn
3d	6.58	6.58	6.58	7.60	7.60	7.60	10.00	10.00	10.00
4s	0.42	0.38	0.27	0.32	0.28	0.27	0.55	0.53	0.53
4p	0.25	0.25	0.26	0.42	0.42	0.42	0.82	0.81	0.80
Q_M	0.75	0.80	0.88	0.65	0.70	0.70	0.63	0.67	0.67

Table 3. Calculated M−N Bond Lengths (R_{M-N}), M−Pc Binding Energies (E_{bind}), Ionization Potentials (IP), and Electron Affinities (EA) in the Ground State of the Systems

		H_{16}PcM	F_{16}PcM	F_{48}PcM[a]
		M = Fe		
R_{Fe-N}, Å		1.916	1.918	1.917
E_{bind}, eV		9.77	9.53	9.95
IP, eV	a_{1u}	6.39 (first)	7.67 (first)	8.76 (first)
	a_{1g}/d_{z^2}	6.42	7.70	10.63
	b_{2g}/d_{xy}	6.58	7.86	9.91
	$1e_g/d_\pi$	7.23	8.48	8.87
	b_{1u}	8.00	8.88	9.75
EA, eV	$1e_g$	−2.55	−3.90	−5.47 (b_{2g})
		M = Co		
R_{Co-N}, Å		1.922	1.924	1.931
E_{bind}, eV		11.51	11.29	11.71
IP, eV	a_{1u}	6.42 (first)	7.69 (first)	8.72 (first)
	$1e_g/d_\pi$	7.19	8.45	9.42
	b_{2g}/d_{xy}	7.51	8.73	9.53
EA, eV	a_{1g}/d_{z^2}	−2.94	−4.26	−5.35
	$2e_g$	−2.09	−3.44	−4.68
		M = Zn		
R_{Zn-N}, Å		2.000	2.001	2.006
E_{bind}, eV		5.64	5.50	5.89
IP, eV	a_{1u}	6.44 (first)	7.70 (first)	8.72 (first)
EA, eV	$2e_g$	−2.18	−3.52	−4.74

[a] Note that the ground state of F_{48}PcFe is different from those of H_{16}PcFe and F_{16}PcFe.

3.1. Cobalt Phthalocyanines. While the peripheral substituents have substantial influence on the electronic structure of the iron phthalocyanines, the Co analogues are much less sensitive. H_{16}PcCo, F_{16}PcCo, and F_{48}PcCo complexes all have a $^2A_{1g}$ ground state, with a fully occupied $1e_g/d_\pi$ level. The ^2E_g state, arising from the $(a_{1g})^2(1e_g)^3$ configuration, lies 0.2−0.3 eV higher in energy. The $^2B_{2g}$ state lies considerably higher, nearly a full eV above the ground state. The $^2E_g - {}^2A_{1g}$ energy gap increases gradually from H_{16}PcCo to F_{16}PcCo to F_{48}PcCo. This comparison between Fe and Co is illustrated more explicitly in Figure 3, where it may be noted first that the metal d-orbitals lie much lower in H_{16}PcCo than in H_{16}PcFe. Unlike the Fe case, the HOMO in PcCo (Pc a_{1u}) is no longer a metal 3d-orbital, and the unoccupied b_{1g} ($d_{x^2-y^2}$) lies below the b_{1u} orbital of the ring.

Similar to H_{16}PcFe, the first ionization of PcCo also occurs from the Pc a_{1u} orbital, and the first IP (6.42 eV) is very close to that obtained for H_{16}PcFe (6.39 eV). The calculated results are in agreement with experimental gas-phase photoelectron spectra (PES) of a series of metal phthalocyanines H_{16}PcM with M = Mg, Fe, Co, Ni, Cu, and Zn,[39] which find a sharp first IP at ∼6.4 eV for all the H_{16}PcMs and conclude that the orbitals of the first ionization are ringlike and not metal 3d-like in all cases. While for H_{16}PcFe the IPs from a_{1u} and a_{1g}/d_{z^2} are very close, for H_{16}PcCo the IP from a_{1u} is 0.77 eV smaller than that from a metal 3d-orbital (d_π), and so the one-electron oxidation of unligated H_{16}PcCo clearly occurs from the Pc ring. On the other hand, electrochemical studies of cobalt phthalocyanines in solution[40,41] find that $PcCo^{II}$ is oxidized to $[PcCo^{III}]^+$; i.e., one-electron oxidation of PcCo occurs from the metal. For example, Lever et al.[40] observed that oxidation of Co^{II} phthalocyanine by halogen (X) leads to the formation of a complex containing the trivalent metal $PcCo^{III}(X)_2$. The disagreement between the calculation and these sorts of experiments may be attributed to the effect of solvent. In solution, the cation species is ligated. The axial ligands raise the energy of the metal a_{1g}/d_{z^2} orbital (see Figure 3) so that the electron in this orbital may be ionized first. Our calculations on $H_{16}PcCo(Py)_2$ (Py = pyridine) show that the first ionization for such a complex indeed occurs from the metal a_{1g}/d_{z^2} orbital (see Table 5). Our further calculations on $H_{16}PcCo(Cl)_2$ show that the latter complex has a ground state of $^2A_{1u}$ $[(1e_g/d_\pi)^4(a_{1u})^1(a_{1g}/d_{z^2})^0]$, where the oxidation state of Co is III, in agreement with experiment;[40,41] a configuration of $(1e_g/d_\pi)^3(a_{1u})^2(a_{1g}/d_{z^2})^0$ is 0.57 eV higher in energy than the ground state.

The similarities between Fe and Co extend (trends are preserved upon fluorination) to the various degrees of fluorosubstitution reported in Table 3. On the other hand, the calculated EAs of PcCo are generally more negative than those of PcFe. For the reduction of PcCo, the added electron goes into the a_{1g}/d_{z^2} orbital, while it enters the $1e_g/d_\pi$ orbital for H_{16}PcFe and F_{16}PcFe. Since F_{48}PcFe has a different electronic structure (as compared to H_{16}PcFe/F_{16}PcFe), the calculated EA of this molecule is even slightly larger (0.12 eV) than that of F_{48}PcCo. The calculated Co−Pc binding energy is significantly larger (∼1.7 eV) than that of Fe−Pc, despite the fact that the Co−N bond lengths are somewhat (0.01 Å) longer than Fe−N. Note that for both Fe and Co, it is the F_{16}PcM species that has the lowest M−Pc binding energy.

The perturbations caused by the Ace ligands in the MO energy diagrams of PcM are illustrated in Figure 3 with $PcFe(Ace)_2$ on the left and $PcCo(Ace)_2$ on the right. The coordination of the two axial ligands lowers the symmetry of the system from D_{4h} to D_{2h} and splits the d_{xz}–d_{yz} degeneracy. Acetone is an electron-donating ligand, shifting the MOs upward. The a_{1g}/d_{z^2} orbital is particularly raised, owing to the strong repulsive interaction between the ligand HOMO and the metal d_{z^2}. As a result, the IPs of $PcM(Ace)_2$ are notably decreased as compared to those of PcM, suggesting that the former will be easier to oxidize than unligated PcM. Unlike $PcFe(Ace)_2$ where the first ionization

Table 4. Calculated Relative Energies (E, eV) for Selected Configurations in $H_{16}PcFe(Ace)_2$, $F_{16}PcFe(Ace)_2$, and $F_{48}PcFe(Ace)_2$

configuration					$E^{relative}$		
d_{xy}	d_{z^2}	d_{yz}	d_{xz}	state[a,b]	$H_{16}PcFe(Ace)_2$	$F_{16}PcFe(Ace)_2$	$F_{48}PcFe(Ace)_2$
2	1	2	1	$^3B_{2g}$ [^3E_g(A)]	**0** (1.933/2.373)[c]	**0** (1.939/2.300)	**0** (1.937/2.279)
2	1	1	2	$^3B_{3g}$ [^3E_g(A)]	0.05 (1.928/2.483)	0.07 (1.932/2.452)	0.09 (1.933/2.405)
1	1	2	2	$^3B_{1g}$ ($^3B_{2g}$)	0.15 (1.925/2.503)	0.18 (1.926/2.468)	0.17 (1.924/2.437)
2	0	2	2	$^1A_{1g}$ ($^1A_{1g}$)	0.16 (1.946/1.969)	0.12 (1.947/1.973)	0.06 (1.942/1.974)

[a] States in parentheses are the corresponding states in unligated species. [b] No minimum or very long Fe−O(Ace) distance was found for the $(d_{xy})^2(d_{z^2})^2(d_{yz})^1(d_{xz})^1$ − $^3B_{1g}$ ($^3A_{2g}$) and $(d_{xy})^1(d_{z^2})^2(d_{yz})^2(d_{xz})^1$ − $^3B_{3g}$ [^3E_g(B)] states. [c] The values in parentheses represent the optimized Fe−N(Pc) and Fe−O(Ace) bond lengths (in Å), respectively.

Table 5. Calculated Properties[a] of $H_{16}PcM$, $F_{16}PcM$, and $F_{48}PcM$ with Two Axial Ligands (L) at the Ground State (M = Fe, Co, Zn; L = Ace, Py)

		$H_{16}PcM(L)_2$ L = Ace	$F_{16}PcM(L)_2$ L = Ace	$F_{48}PcM(L)_2$ L = Ace	$H_{16}PcCo(L)_2$ L = Py
		M = Fe			
$R_{M-N(Pc)}$ (Å)		1.933	1.939	1.937	
$R_{M-O(Ace)}$ (Å)		2.373	2.300	2.279	
E_{bind}[PcM-$(L)_2$] (eV)		0.25	0.63	0.94	
Q_M (e)		0.79	0.81	0.80	
Q_{Ace} (e)		0.15	0.19	0.22	
IP (eV)	a_{1g}/d_{z^2}	6.97	8.01	8.86	
	$1b_{3g}/d_{yz}$	**5.74** (first)	**6.99** (first)	**7.94** (first)	
	b_{1g}/d_{xy}	6.01	7.26	8.14	
	a_{1u}	6.00	7.21	8.27	
EA (eV)	$1b_{2g}/d_{xz}$	−2.29	−3.55	−4.72	
	$2b_{3g}$	−1.66	−2.96	−4.22	
		M = Co			
$R_{M-N(Pc)}$ (Å)		1.926	1.929	1.932 (1.924)[c]	1.934
$R_{M-O(Ace)}$ (Å)		2.401	2.366	2.331 (2.314)	2.318
E_{bind}[PcM-$(L)_2$] (eV)		0.16	0.49	1.06	0.77
Q_M (e)		0.67	0.70	0.69	0.90
Q_{Ace} (e)		0.13	0.14	0.16	0.18
IP (eV)	a_{1g}/d_{z^2}	7.56	8.69	9.45	**5.85** (first)
	a_{1u}	**6.03** (first)	**7.25** (first)	**8.31** (first)	6.11
EA (eV)	$2b_{3g}$	−1.67	−2.98	−4.25	−1.82
	a_{1g}/d_{z^2}	−1.63	−2.82	−3.87	−0.95
E_{dis}[d](eV)		−1.11	−0.79	−0.33	−0.39
		M = Zn			
$R_{M-N(Pc)}$ (Å)		2.010	2.014	2.012 (2.006)[c]	
$R_{M-O(Ace)}$ (Å)		2.505	2.459	2.414 (2.411)	
E_{bind}[PcM-$(L)_2$] (eV)		0.12	0.44	0.73	
Q_M (e)		0.64	0.67	0.65	
Q_{Ace} (e)		0.10	0.12	0.13	
IP (eV)	a_{1u}	**6.05** (first)	**7.26** (first)	**8.30** (first)	
EA (eV)	$2b_{3g}$	−1.78	−3.08	−4.32	

[a] R: distance, E_{bind}[PcM-$(Ace)_2$]: binding energy between PcM and two Ace ligands, Q: charge distribution, IP: ionization potential, EA: electron affinity. [b] The first IP is indicated in bold. [c] The values in parentheses are experimental distances for $F_{64}PcM(Ace)_2$ (refs 14 and 15). [d] Dissociation energy for $[PcCo(L)_2]^-$ → $[PcCo]^-$ + 2L.

occurs from the central metal ($1b_{3g}/d_{yz}$), Table 5 reveals that of $PcCo(Ace)_2$ takes place still from the Pc a_{1u} orbital, similar to unligated PcM. As mentioned above, in the presence of relatively strong field ligands L (e.g. L = Py), the first ionization of $PcCo(L)_2$ takes place from the central metal. For $PcCo(Ace)_2$, the IP from a_{1g}/d_{z^2} is more than 1 eV larger than that from a_{1u}. There is about a 0.4 eV decrease of IP from PcCo to $PcCo(Ace)_2$, in contrast to ∼0.8 eV decrease of IP from PcFe to $PcFe(Ace)_2$. Note also that for any degree of substitution, the IP of the $PcCo(Ace)_2$ is roughly 0.3 eV higher than the corresponding quantity for the Fe analogue.

The axial ligands reduce the electron affinity of PcM considerably (by 1.1−1.3 eV) when M is Co. In contrast to PcCo, the added electron in $PcCo(Ace)_2$ now occupies a high-lying antibonding Pc $2b_{3g}$ orbital. Since the added electron in PcCo goes into a low-lying metal orbital, $[PcCo]^-$ has a relatively low energy. Unless the ligand field of L is very strong, the $[PcM(L)_2]^-$ complex is expected to be unstable

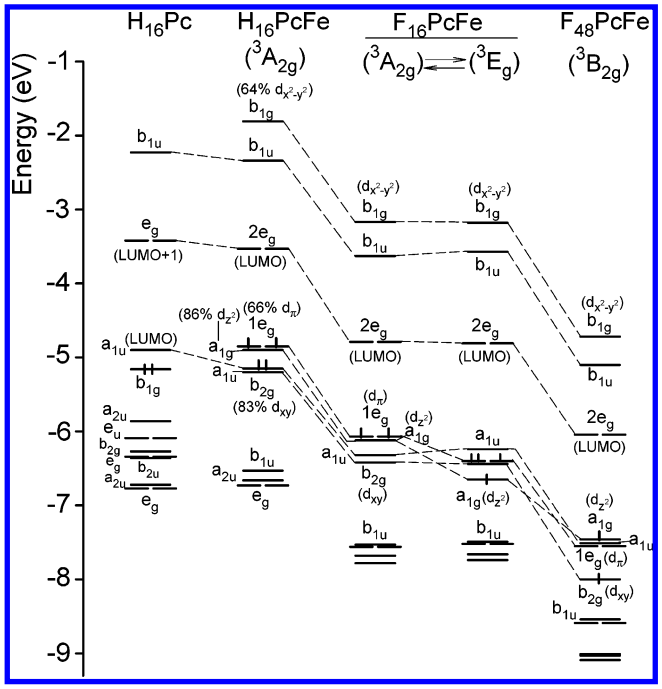

Figure 2. Orbital energy levels of $H_{16}Pc$ (on left, with no H atoms in the ring cage) and the various iron phthalocyanines.

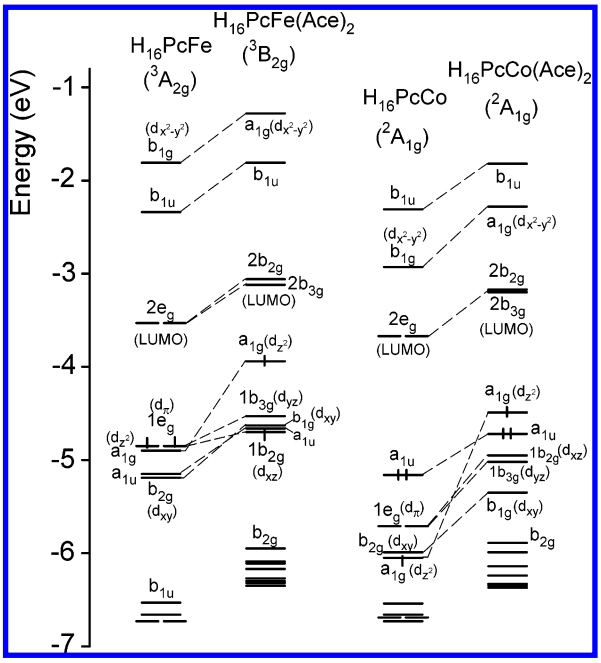

Figure 3. Orbital energy levels of $H_{16}PcM$ (M = Fe, Co) when complexed with two axial acetone (Ace) ligands.

and to dissociate into $[PcCo]^- + 2L$. Our calculations show that the dissociation energy E_{dis} for $[H_{16}PcCo(Ace)_2]^-$ is strongly exothermic (by more than 1 eV). This may account for the fact that previous experiments[41,42] have always detected Co^I and no Co^{II} when cobalt phthalocyanines are reduced. We note that the EA to the $2b_{3g}$ orbital is not significantly larger than that to a_{1g}/d_{z^2}, especially for $H_{16}PcCo(Ace)_2$. When a_{1g}/d_{z^2} is doubly occupied, the two electrons in this orbital would result in a very strong repulsion to axial ligands. This small difference in EA between $2b_{3g}$ and a_{1g}/d_{z^2} also leads us to expect that $[PcM(L)_2]^-$ is unstable

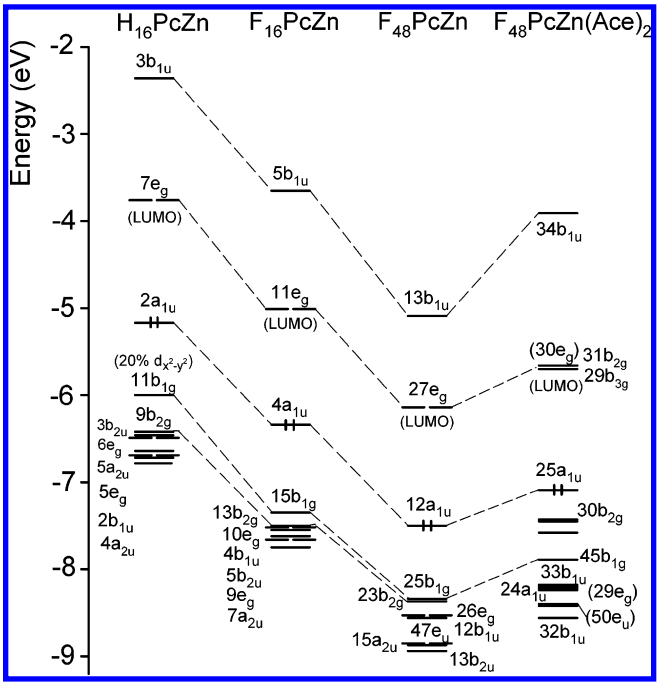

Figure 4. Orbital energy levels of the various zinc phthalocyanines.

and will dissociate. In fact, E_{dis} decreases to −0.33 eV when the $-C_2F_5$ substituents are introduced on the Pc ring. From the calculated E_{dis} value for $[H_{16}PcCo(Py)_2]^-$ (−0.39 eV) and the trend in E_{dis} from $[H_{16}PcCo(Ace)_2]^-$ to $[F_{48}PcCo(Ace)_2]^-$, the $[F_{48}PcCo(Py)_2]^-$ complex is expected to be stable against dissociation.

For both PcFe and $PcFe(Ace)_2$, however, the EAs all correspond to the addition of an electron to a low-lying metal d-orbital, and so there is a smaller decrease of EA from PcFe to $PcFe(Ace)_2$ as compared to the cobalt systems.

The binding energy (E_{bind}) between $H_{16}PcCo$ and a pair of Ace molecules is rather small, 0.16 eV. This quantity rises to more than 1 eV for the heavily substituted $F_{48}PcCo$. Corresponding to the increase of E_{bind}, the Co−O(Ace) distance is shortened as more F-atoms are added to the system. The Co−N(Pc) and Co−O(Ace) bond lengths (1.932 Å, 2.331 Å) calculated in $F_{48}PcCo(Ace)_2$ are in excellent agreement with the X-ray structural data on $F_{64}PcCo(Ace)_2$ (1.924 Å, 2.314 Å).[15] The axial ligation does not affect the equatorial Co−N distance very much (<0.005 Å).

3.2. Zinc Phthalocyanines. *3.2.1. Electronic Structure and Properties.* The perturbations in the orbital levels that accompany the various changes in the Zn systems are illustrated in Figure 4. The 3d-orbitals are particularly low in energy for Zn; b_{1g} has lost all but 20% of its metal contribution and is largely Pc σ in character. As was true for the Fe systems in Figure 2, fluorosubstitution has a strong lowering effect on the MOs. The magnitude of this shift is quite uniform for most MOs including the HOMO and LUMO. The main exceptions are some orbitals below the HOMO-1. For instance, the energy gap between b_{1g} (HOMO-1) and b_{2g} (HOMO-2) is large in $H_{16}PcZn$ but nearly disappears in $F_{48}PcZn$.

The first oxidation of PcZn clearly leads to a π-cation radical, where the electron is removed from the HOMO a_{1u},

yielding a $^2A_{1u}$ ground state. This IP is strikingly similar in magnitude to the Co cases. In the case of reduction, the electron is accommodated in the LUMO e_g (Pc π^*). Both IP and EA are increased considerably by the $-C_2F_5$ substituents, in agreement with the trend in the electrochemical oxidation and reduction potentials.[13] The EA values are slightly more negative for the Zn molecules than for Co.

With two electrons in the b_{1g} ($d_{x^2-y^2}$) orbital in PcZn, the repulsive interaction between these electrons and those on the pyrrole nitrogens lengthens the M−N bond length by ∼0.08 Å relative to Co and considerably decreases the M−Pc binding energy, as is evident by the E_{bind} entries in Table 3 for M = Zn.

On the other hand, the presence of two electrons in the a_{1g}/d_{z^2} orbital in PcZn(Ace)$_2$ gives rise to longer axial Zn−O(Ace) bond lengths as compared to Co−O(Ace). Therefore the binding energy of PcZn−(Ace)$_2$ is smaller than the PcCo−(Ace)$_2$ value. Also, there is a large increase of the PcZn−(Ace)$_2$ binding energy when more F atoms are added to the system. It was argued that the perfluoro peripheral substituents withdraw electron density from the inner ring and the central metal so that the axial ligation of F_{64}PcZn is enhanced relative to the parent H_{16}PcZn complex.[13] According to the calculation, the presence of the F-atoms in F_{16}-PcZn makes the atomic charge on Zn more positive by 0.04 (see Table 2), but no change in Q_M is found from F_{16}PcZn to F_{48}PcZn. The same is true for the cobalt systems. There is a more pronounced shortening of the axial M−O(Ace) bond distance from H_{16}PcZn to F_{48}PcZn than from H_{16}PcCo to F_{48}PcCo. Again the calculated bond lengths $R_{Zn-N(Pc)}$ = 2.012 Å and $R_{Zn-O(Ace)}$ = 2.414 Å in F_{48}PcZn agree very well with the 2.006 Å and 2.411 Å measured in the F_{64}-PcZn crystal.[14] An addition of (Ace)$_2$ to PcZn produces little geometric change, similar to the PcCo case.

The MO levels are shifted up from F_{48}PcZn to F_{48}PcZn-(Ace)$_2$. The increase in the energy of a_{1u} leads to a relatively small IP from this orbital. Therefore, solvent coordination to the central metal is able to decrease the oxidation potential of PcM, as observed experimentally.[13] While attempts to oxidize F_{64}PcZn were unsuccessful, there is evidence that in the presence of strong electron-donating ligands such as imidazole, F_{64}PcZn can oxidized electrochemically.[13] The experimental observation can be accounted for by the calculated results. Here the IP and EA of PcZn(Ace)$_2$ are about 0.4 eV smaller (lower) than those of PcZn.

3.2.2. Electronic Spectra. Electronic spectra of both H_{16}-PcZn and F_{48}PcZn have been calculated using the semiempirical ZINDO method,[13] with the aim of understanding the changes in energy of the spectral features when the electron-withdrawing peripheral substituents ($-C_2F_5$) are introduced. However, the semiempirical method yields some excitation energies which are considerably too large (more than 1 eV) as compared to the experimental spectra. In this study, we describe the results of TDDFT calculations for the series of PcZn complexes from H_{16}PcZn to F_{16}PcZn to F_{48}PcZn to F_{48}PcZn(Ace)$_2$. Our calculated excitation energies and oscillator strengths for several lowest, spin-allowed singlet ^1E_u excited states are displayed in Table 6, together with available experimental data.[13,33]

The experimental spectrum of PcZn is characterized by an intense absorption band in the visible (Q-band) and two other strong absorption bands in the near-UV (B_1 and B_2 bands).[33] The multiple bands in the B region is supported by the calculations. The Q-band is assigned to the 1^1E_u state, which is nearly pure (90%) HOMO → LUMO transition. For H_{16}PcZn, 1^1E_u is calculated to be 1.96 eV, in good agreement with the experimental value of 1.85 eV.[33] The close-lying 6^1E_u and 7^1E_u states are responsible for the B_2 and B_1 bands, respectively; their oscillator strengths are both quite large. Different from 1^1E_u, the latter two states involve significant mixture of several transitions. Again, the calculated E^{exc} values (3.40 and 3.74 eV) for the B bands agree very well with experiment (3.16 and 3.71 eV).[33] The same is true for F_{48}PcZn.

The 1^1E_u state (Q-band) in F_{16}PcZn is predicted at 1.84 eV, a red shift of 0.12 eV relative to that of H_{16}PcZn. For the B bands, the red shift is somewhat larger, about 0.2 eV. These results reveal that the introduction of the electron-withdrawing F-atoms into the Pc ring shifts the Q and B bands to the red.

Turning to F_{48}PcZn, its 1^1E_u has nearly the same E^{exc} as that of F_{16}PcZn. So the partial replacement of eight F-atoms by eight $-C_2F_5$ groups does not shift the Q-band. Here the main effect of the $-C_2F_5$ substituents is a notable red shift of the B_1 band.

From F_{48}PcZn to F_{48}PcZn(Ace)$_2$, the E^{exc} values for the various ^1E_u states remain nearly unchanged, indicating that the presence of axial acetone ligands does not change the positions of the absorption bands. These results are also in accord with experimental observations.[13] Note that in Figure 4, the LUMO−HOMO energy gap is not shown to be changed from one system to another, but the peripheral substituents may still change the calculated E^{exc} for the HOMO → LUMO transition. This is because the 1^1E_u state is not a pure HOMO → LUMO transition; it contains some contributions (∼10%) from other transitions owing to configuration interaction. As a matter of fact, the change in E^{exe} is insignificant from one system to another.

Similar to the calculations on H_{16}PcNi by Rosa et al.,[31] our TDDFT calculations on PcZn also predict several allowed $\pi \rightarrow \pi^*$ transitions located between the Q and B bands. These $\pi \rightarrow \pi^*$ transitions may be responsible for the intensity and broadness of the B bands. The ZINDO calculations predicted a HOMO → LUMO+1 transition (called second $\pi \rightarrow \pi^*$ transition) located to the red of the B band for both H_{16}PcZn and F_{48}PcZn. Our results show that the HOMO → LUMO+1 transition is located to the blue of the B band for F_{48}PcZn. No analogous transition is found for F_{16}PcZn.

3.2.3. PcZn(Cl) and PcZn(Cl$^-$) Complexes. Finally, calculations were also performed on the various PcZn(Cl) and PcZn(Cl$^-$) complexes. When only a single axial ligand is attached to the system, significant out-of-plane displacement of the metal is expected and in fact observed. For each molecule, the geometry was optimized assuming C_{4v} symmetry. The calculated PcZn-L binding energies (L = Cl, Cl$^-$) and three critical coordination parameters in PcZn(L) are displayed in Table 7. $R_{Ct\cdots N}$ (distance between the center of the ring and pyrrole nitrogen atom) is a measure of the ring

Table 6. Calculated Excitation Energies (E^{exc}, in eV) and Oscillator Strengths (f)

system	state	contribution[a]	E^{exc}, eV calcd	E^{exc}, eV exptl[c]	f	assignment
$H_{16}PcZn$	1^1E_u	91% ($2a_{1u} \rightarrow 7e_g$)	1.96	1.85	0.6482	Q
	2^1E_u	97% ($3b_{2u} \rightarrow 7e_g$)	2.80		0.0280	$\pi \rightarrow \pi^*$
	3^1E_u	39% ($2b_{1u} \rightarrow 7e_g$); 33% ($5a_{2u} \rightarrow 7e_g$); 25% ($5a_{2u} \rightarrow 7e_g$)	3.02		0.0014	$\pi \rightarrow \pi^*$
	4^1E_u	54% ($2b_{1u} \rightarrow 7e_g$); 23% ($4a_{2u} \rightarrow 7e_g$); 18% ($5a_{2u} \rightarrow 7e_g$)	3.07		0.3390	$\pi \rightarrow \pi^*$
	5^1E_u	76% ($2a_{1u} \rightarrow 8e_g$)	3.35		0.0242	$\pi \rightarrow \pi^*$
	6^1E_u	36% ($1a_{1u} \rightarrow 7e_g$); 23% ($4a_{2u} \rightarrow 7e_g$); 18% ($2a_{1u} \rightarrow 8e_g$); 17% ($5a_{2u} \rightarrow 7e_g$)	3.40	3.16	0.6840	B_2
	7^1E_u	53% ($1a_{1u} \rightarrow 7e_g$); 17% ($4a_{2u} \rightarrow 7e_g$); 16% ($5a_{2u} \rightarrow 7e_g$)	3.74	3.71	1.0402	B_1
	8^1E_u	95% ($6e_g \rightarrow 3b_{1u}$)	4.22		0.0332	
$F_{16}PcZn$	1^1E_u	91% ($4a_{1u} \rightarrow 11e_g$)	1.84		0.6332	Q
	2^1E_u	84% ($4b_{1u} \rightarrow 11e_g$); 11% ($5b_{2u} \rightarrow 11e_g$)	2.60		0.1442	$\pi \rightarrow \pi^*$
	3^1E_u	87% ($5b_{2u} \rightarrow 11e_g$); 10% ($4b_{1u} \rightarrow 11e_g$)	2.71		0.1360	$\pi \rightarrow \pi^*$
	4^1E_u	80% ($7a_{2u} \rightarrow 11e_g$); 15% ($6a_{2u} \rightarrow 11e_g$)	2.88		0.2928	$\pi \rightarrow \pi^*$
	5^1E_u	67% ($3a_{1u} \rightarrow 11e_g$); 29% ($6a_{2u} \rightarrow 11e_g$)	3.16		0.1038	B_2
	6^1E_u	43% ($6a_{2u} \rightarrow 11e_g$); 23% ($3a_{1u} \rightarrow 11e_g$)	3.58		1.4316	B_1
	7^1E_u	83% ($10e_g \rightarrow 5b_{1u}$)	4.00		0.0220	
	8^1E_u	89% ($9e_g \rightarrow 5b_{1u}$)	4.15		0.0786	
$F_{48}PcZn$	1^1E_u	91% ($12a_{1u} \rightarrow 27e_g$)	1.83	1.80	0.7984	Q
	2^1E_u	95% ($12b_{1u} \rightarrow 27e_g$)	2.51		0.3138	$\pi \rightarrow \pi^*$
	3^1E_u	75% ($13b_{2u} \rightarrow 27e_g$); 13% ($11a_{1u} \rightarrow 27e_g$)	2.89		0.1374	$\pi \rightarrow \pi^*$
	4^1E_u	59% ($11a_{1u} \rightarrow 27e_g$); 22% ($13b_{2u} \rightarrow 27e_g$); 17% ($15a_{2u} \rightarrow 27e_g$)	2.95		0.0086	$\pi \rightarrow \pi^*$
	5^1E_u	91% ($14a_{2u} \rightarrow 27e_g$)	3.13	2.89	0.0124	B_2
	6^1E_u	48% ($15a_{2u} \rightarrow 27e_g$); 20% ($12a_{1u} \rightarrow 28e_g$); 12% ($11a_{1u} \rightarrow 27e_g$)	3.33	3.10	1.7998	B_1
	7^1E_u	62% ($12a_{1u} \rightarrow 28e_g$); 27% ($26e_g \rightarrow 13b_{1u}$)	3.41		0.0356	$\pi \rightarrow \pi^*$
	8^1E_u	60% ($26e_g \rightarrow 13b_{1u}$); 12% ($12a_{1u} \rightarrow 28e_g$)	3.62		0.0058	
	9^1E_u	70% ($25e_g \rightarrow 13b_{1u}$); 22% ($12a_{1u} \rightarrow 29e_g$)	4.02		0.0700	
$F_{48}PcZn(Ace)_2$[b]	1^1E_u	90% ($25a_{1u} \rightarrow 30e_g$)	1.87		0.8075	Q
	2^1E_u	91% ($24a_{1u} \rightarrow 30e_g$)	2.65		0.2024	$\pi \rightarrow \pi^*$
	3^1E_u	62% ($33b_{1u} \rightarrow 30e_g$); 22% ($23a_{1u} \rightarrow 30e_g$)	2.86		0.5055	$\pi \rightarrow \pi^*$
	4^1E_u	89% ($32b_{1u} \rightarrow 30e_g$)	2.99		0.0021	$\pi \rightarrow \pi^*$
	5^1E_u	56% ($23a_{1u} \rightarrow 30e_g$); 27% ($31b_{1u} \rightarrow 30e_g$)	3.13		0.1025	B_2
	6^1E_u	51% ($25a_{1u} \rightarrow 31e_g$); 38% ($31b_{1u} \rightarrow 30e_g$)	3.30		0.7449	B_1
	7^1E_u	41% ($25a_{1u} \rightarrow 31e_g$); 28% ($31b_{1u} \rightarrow 30e_g$)	3.37		0.3465	$\pi \rightarrow \pi^*$
	8^1E_u	75% ($28e_g \rightarrow 26a_{1u}$)	3.59		0.1101	

[a] Contribution of less than 10% is not listed. [b] For convenience, we also use the label e_g (of D_{4h} symmetry) for the lower symmetry system. [c] References 13 and 33.

Table 7. Calculated Properties of $H_{16}PcZn$, $F_{16}PcZn$, and $F_{48}PcZn$ with Axial Ligands of Cl and of Cl^-

	$H_{16}PcZn(Cl)$	$F_{16}PcZn(Cl)$	$F_{48}PcZn(Cl)$	$H_{16}PcZn(Cl^-)$	$F_{16}PcZn(Cl^-)$	$F_{48}PcZn(Cl^-)$
$R_{Ct\cdots N(Pc)}$[a] (Å)	1.976	1.971	1.978	1.987	1.986	1.986
$R_{Ct\cdots Zn}$[b] (Å)	0.761	0.774	0.736	0.710	0.695	0.695
R_{Zn-Cl} (Å)	2.232	2.214	2.200	2.269	2.250	2.249
Q_{Zn} (e)	0.54	0.54	0.52	0.57	0.56	0.55
Q_{Cl} (e)	−0.45	−0.41	−0.44	−0.51	−0.45	−0.44
$E_{bind}(PcZn-Cl)$[c] (eV)	1.77	1.62	1.32	1.81	2.96	3.79

[a] Ct denotes the center of the Pc ring and $R_{Ct\cdots N(Pc)}$ denotes the distance between Ct and N(Pc). [b] $R_{Ct\cdots Zn}$ denotes displacement of the Zn atom out of the Pc plane. [c] Binding energy between PcZn and Cl or Cl^-.

core size, $R_{Ct\cdots Zn}$ represents the displacement of the Zn atom out of the N_4-plane toward the L ligand, and R_{Zn-Cl} refers to the Zn−Cl bond length.

The calculated $H_{16}PcZn-Cl$ binding energy E_{bind} is large, 1.77 eV, indicating a high affinity of $H_{16}ZnPc$ for Cl. As an electron-withdrawing ligand, the binding of neutral Cl to F_{48}-PcZn becomes significantly weaker. A large Zn out-of-plane displacement is found when Cl is coordinated to the system. In this case, the Ct···N distance becomes somewhat shorter than R_{Zn-N} of unligated PcZn.

For the chloride ion, there is a clear trend of increasing binding energy in the order $H_{16}PcZn-Cl^- < F_{16}PcZn-Cl^-$

< $F_{48}PcZn-Cl^-$, where the $F_{48}PcZn-Cl^-$ binding energy is much larger than that of $H_{16}PcZn-Cl^-$. The values of E_{bind} correlate well with the relative stabilities of these PcZn(Cl^-) complexes.[13]

4. Conclusions

The following main conclusions may be drawn from the calculated results.

(1) While the strongly electron-withdrawing $-C_2F_5$ groups on the Pc ring are able to change the ground state of PcFe, they do not influence the ground state of PcCo.

(2) Corresponding to the downshifts of the valence MOs caused by the peripheral substituents, the first ionization potential (IP) is increased by ~1.3 eV from H_{16}PcM to F_{16}PcM and by another ~1.1 eV from F_{16}PcM to F_{48}PcM. A similar increase in the EA is also found on going from H_{16}PcM to F_{48}PcM. These results account for the fact that the F_{64}PcM compounds are difficult to oxidize but easy to reduce.[13] The change from H_{16}PcZn to F_{48}PcZn does not produce an obvious change in the LUMO−HOMO energy gap, but large changes in the relative MO energies are found between the b_{1g} (HOMO-1) and b_{2g} (HOMO-2) orbitals.

(3) The axial acetone (Ace) ligands in PcM$(Ace)_2$ shift the MO energy levels upward. There is a decrease of ~0.8 eV in IP from PcFe to PcFe$(Ace)_2$, and a decrease of ~0.4 eV when the metal M is Co and Zn. Therefore, axial coordination by (strong) σ-donors renders easier the oxidation of the compound, as observed experimentally.[13]

(4) The calculated H_{16}PcM-$(Ace)_2$ binding energy (E_{bind}) is small (<0.2 eV), particularly for M = Zn, indicating a low affinity of the parent metal phthalocyanine for acetone. The E_{bind} is increased to nearly 1 eV when the $-C_2F_5$ groups are introduced at the periphery of the Pc ring. This rise accounts for the experimental result[13] that there is formation of a F_{64}PcZn$(Ace)_2$ compound, but no H_{16}PcZn$(Ace)_2$ was detected. On the other hand, the calculated PcZn$-Cl^-$ binding energies can also account for the relative stabilities of those PcZn(Cl^-) compounds.

(5) The TDDFT calculated excitation energies for the PcZn complexes are in quantitative agreement with available experimental data. The substitution of 16 H-atoms in H_{16}PcZn by F-atoms (i.e. from H_{16}PcZn to F_{16}PcZn) shifts the Q and B bands to the red. A further red shift in the B_1 band occurs with partial replacement of eight F-atoms in F_{16}PcZn by $-C_2F_5$ groups, but there is no shift in the Q-band from F_{16}PcZn to F_{48}PcZn. On the other hand, the calculated electronic spectrum of F_{48}PcZn is nearly the same as that of F_{48}PcZn$(Ace)_2$, supporting an assumption that the results (spectra) for the fluorinated phthalocyanines are virtually independent of the presence or absence of axial ligands.[13]

(6) The calculated redox properties of gas-phase cobalt phthalocyanines may be different from those measured in solution. These differences are likely due to association of specific solvent molecules with the complex.

Acknowledgment. This work was supported by grant DAAD19-99-1-0206 (to S.S.) from the Army Research Office and by grant S06 GM08047 from the National Institutes of Health (to M.J.H. and J.D.W.).

References

(1) Simon, J.; Andre, J.-J. *Molecular Semiconductors*; Springer: Berlin, 1985.

(2) Tang, C. W. *Appl. Phys. Lett.* **1986**, *48*, 183−185.

(3) Loutfy, R. O.; Hor, A. M.; Hsiao, C. K.; Baranyi, G.; Kazmaier, P. *Pure Appl. Chem.* **1988**, *60*, 1047−1054.

(4) Kato, M.; Nishioka, Y.; Kaifu, K.; Kawamura, K.; Ohno, S. *Appl. Phys. Lett.* **1985**, *46*, 196−197.

(5) Temofonte, T.; Schoch, K. F. *J. Appl. Phys.* **1989**, *65*, 1350−1355.

(6) Marks, T. J. *Angew. Chem., Int. Ed. Engl.* **1990**, *29*, 857−879.

(7) Toshima, N.; Tominage, T. *Bull. Chem. Soc. Jpn.* **1996**, *69*, 2111−2122.

(8) Palacin, S.; Lesieur, P.; Stefanelli, I.; Barraud, A. *Thin Solid Films* **1988**, *159*, 83−90.

(9) Simon, J.; Sirlin, C. *Pure Appl. Chem.* **1989**, *61*, 1625−1629.

(10) Gasstevens, M. K.; Samoc, M.; Pfleger, J.; Prasad, P. N. *J. Chem. Phys.* **1990**, *92*, 2019−2024.

(11) Mckeown, N. B. *Phthalocyanine Materials*; Cambridge University Press: Cambridge, 1998.

(12) *Phthalocyanines: Properties and Applications*; Leznoff, C. C., Lever, A. B. P., Eds.; VCH Publishers: New York, 1996; Vol. 4.

(13) Keizer, S. P.; Mack, J.; Bench, B. A.; Gorun, S. M.; Stillman, M. J. *J. Am. Chem. Soc.* **2003**, *125*, 7067−7085.

(14) Bench, B. A.; Beveridge, A.; Sharman, W. M.; Diebold, G. J.; van Lier, J. E.; Gorun, S. M. *Angew. Chem., Int. Ed.* **2002**, *41*, 748−750.

(15) Bench, B. A.; Brennessel, W. W.; Lee, H.-J.; Gorun, S. M. *Angew. Chem., Int. Ed.* **2002**, *41*, 750−754.

(16) Lee, H.-J.; Brennessel, W. W.; Brucker, W. J.; Lessing, J. A.; Young, V. G., Jr.; Gorun, S. M. To be submitted.

(17) Liao, M.-S.; Kar, T.; Gorun, S. M.; Scheiner, S. *Inorg. Chem.* **2004**, *43*, 7151−7161.

(18) Baerends, E. J.; Ellis, D. E.; Roos, P. *Chem. Phys.* **1973**, *2*, 41−51.

(19) Versluis, L.; Ziegler, T. *J. Chem. Phys.* **1988**, *88*, 322−328.

(20) te Velde, G.; Baerends, E. J. *J. Comput. Phys.* **1992**, *99*, 84−98.

(21) Fonseca-Guerra, C.; Snijders, J. G.; te Velde, G.; Baerends, E. J. *Theor. Chem. Acc.* **1998**, *99*, 391−403.

(22) Liao, M.-S.; Scheiner, S. Unpublished results.

(23) Vosko, S. H.; Wilk, L.; Nusair, M. *Can. J. Phys.* **1980**, *58*, 1200−1211.

(24) Becke, A. D. *Phys. Rev. A* **1988**, *38*, 3098−3100.

(25) Perdew, J. P. *Phys. Rev. B* **1986**, *33*, 8822−8824.

(26) Johnson, B. G.; Gill, P. M. W.; Pople, J. A. *J. Chem. Phys.* **1993**, *98*, 5612−5626.

(27) Li, J.; Schreckenbach, G.; Ziegler, T. *J. Am. Chem. Soc.* **1995**, *117*, 486−494.

(28) Ziegler, T.; Tschinke, V.; Baerends, E. J.; Snijders, J. G.; Ravenek, W. *J. Phys. Chem.* **1989**, *93*, 3050−3056.

(29) van Gisbergen, S. J. A.; Snijders, J. G.; Baerends, E. J. *Comput. Phys. Commun.* **1999**, *118*, 119−138.

(30) Nguyen, K. A.; Pachter, R. *J. Chem. Phys.* **2001**, *114*, 10757−10767.

(31) Rosa, A.; Ricciardi, G.; Baerends, E. J.; van Gisbergen, S. J. A. *J. Phys. Chem. A* **2001**, *105*, 3311−3327.

(32) (a) Kahl, J. L.; Faulkner, L. R.; Dwarakanath, K.; Tachikawa, H. *J. Am. Chem. Soc.* **1986**, *108*, 5434−5440. (b) Williamson, B. E.; VanCott, T. C.; Boyle, M. E.; Misener, G. C.; Stillman, M. J.; Schatz, P. N. *J. Am. Chem. Soc.* **1992**, *114*, 2412−2419. (c) Janczak, J.; Kubiak, R. *Inorg. Chim. Acta* **2003**, *342*, 64−76.

(33) Stillman, M. J.; Nyokong, T. In *Phthalocyanine: Principles and Properties*; Leznoff, C. C., Lever, A. B. P., Eds.; VCH Publishers: New York, 1993; Vol. 1, Chapter 3, pp 133−290.

(34) Dale, B. W.; Williams, R. J. P. *J. Chem. Phys.* **1968**, *49*, 3445−3449.

(35) Barraclough, C. G.; Martin, R. L.; Mitra, S. *J. Chem. Phys.* **1970**, *53*, 1643−1648.

(36) Stillman, M. J.; Thomson, A. J. *J. Chem. Soc., Faraday Trans. 2* **1974**, *70*, 790−804.

(37) Liao, M.-S.; Scheiner, S. *J. Chem. Phys.* **2001**, *114*, 9780−9791.

(38) The calculated results of the iron phthalocyanines with the present version of the ADF program may be slightly different from those obtained with an older version,[17] but the trends remain unchanged.

(39) Berkowitz, J. *J. Chem. Phys.* **1979**, *70*, 2819−2828.

(40) Myers, J. F.; Canham, G. W. R.; Lever, A. B. P. *Inorg. Chem.* **1975**, *14*, 461−468.

(41) Minor, P. C.; Gouterman, M.; Lever, A. B. P. *Inorg. Chem.* **1985**, *24*, 1894−1900.

(42) Clack, D. W.; Yandle, J. R. *Inorg. Chem.* **1972**, *11*, 1738−1742.

CT050105Y